

# cAMP-independent DNA binding of the CRP family protein Ddrl from *Deinococcus radiodurans*

Yudong Wang,<sup>1</sup> Jing Hu,<sup>1</sup> Xufan Gao,<sup>2</sup> Yuchen Cao,<sup>1</sup> Shumai Ye,<sup>1</sup> Cheng Chen,<sup>1</sup> Liangyan Wang,<sup>1</sup> Hong Xu,<sup>1</sup> Miao Guo,<sup>1</sup> Dong Zhang,<sup>1,2</sup> Ruhong Zhou,<sup>1,2,3,4</sup> Yuejin Hua,<sup>1</sup> Ye Zhao<sup>1</sup>

**AUTHOR AFFILIATIONS** See affiliation list on p. 16.

**ABSTRACT** The cAMP receptor proteins (CRPs) play a critical role in bacterial environmental adaptation by regulating global gene expression levels via cAMP binding. Here, we report the structure of Ddrl, a CRP family protein from *Deinococcus radiodurans*. Combined with biochemical, kinetic, and molecular dynamics simulations analyses, our results indicate that Ddrl adopts a DNA-binding conformation in the absence of cAMP and can form stable complexes with the target DNA sequence of classical CRPs. Further analysis revealed that the high-affinity cAMP binding pocket of Ddrl is partially filled with Tyr113-Arg55-Glu65 sidechains, mimicking the anti-cAMP-mediated allosteric transition. Moreover, the second syn-cAMP binding site of Ddrl at the protein-DNA interface is more negatively charged compared to that of classical CRPs, and manganese ions can enhance its DNA binding affinity. Ddrl can also bind to a target sequence that mimics another transcription factor, DdrO, suggesting potential cross-talk between these two transcription factors. These findings reveal a class of CRPs that are independent of cAMP activation and provide valuable insights into the environmental adaptation mechanisms of *D. radiodurans*.

**IMPORTANCE** Bacteria need to respond to environmental changes at the gene transcriptional level, which is critical for their evolution, virulence, and industrial applications. The cAMP receptor protein (CRP) of *Escherichia coli* (ecCRP) senses changes in intracellular cAMP levels and is a classic example of allosteric effects in textbooks. However, the structures and biochemical activities of CRPs are not generally conserved and there exist different mechanisms. In this study, we found that the proposed CRP from *Deinococcus radiodurans*, Ddrl, exhibited DNA binding ability independent of cAMP binding and adopted an apo structure resembling the activated CRP. Manganese can enhance the DNA binding of Ddrl while allowing some degree of freedom for its target sequence. These results suggest that CRPs can evolve to become a class of cAMP-independent global regulators, enabling bacteria to adapt to different environments according to their characteristics. The first-discovered CRP family member, ecCRP (or CAP) may well not be typical of the family and be very different to the ancestral CRP-family transcription factor.

**KEYWORDS** transcription factor, DNA binding, dimer, cAMP, allosteric effect, microscale thermophoresis

**G**lucose is the preferred carbon source in *Escherichia coli*. Early studies on *E. coli* lacking glucose during growth led to the discovery of elevated levels of the intracellular signaling molecule cyclic 3',5'-AMP (cAMP), which activates the DNA binding of the cAMP receptor protein (CRP) and regulates global gene expression of more than 7% of genes. This phenomenon is known as catabolite repression, enabling bacteria to utilize non-preferred carbon sources such as lactose (1, 2). Later, bacterial CRPs have

**Editor** Paul Babitzke, The Pennsylvania State University, University Park, Pennsylvania, USA

Address correspondence to Ye Zhao, [yezhao@zju.edu.cn](mailto:yezhao@zju.edu.cn).

The authors declare no conflict of interest.

See the funding table on p. 16.

**Received** 14 April 2024

**Accepted** 30 May 2024

**Published** 25 June 2024

Copyright © 2024 Wang et al. This is an open-access article distributed under the terms of the [Creative Commons Attribution 4.0 International license](https://creativecommons.org/licenses/by/4.0/).

been shown to be involved in a wider range of regulatory effects related to environmental adaptation, such as quorum sensing (3), iron acquisition (4), virulence (5), and motility (6). Moreover, CRPs may also play a non-transcriptional regulatory role in some bacteria (7, 8). For example, cAMP-CRP is hypothesized to be required for *Shewanella putrefaciens* biofilm maintenance through physical interaction with BpfD (8).

*E. coli* CRP (ecCRP) was the first transcription factor with a crystal structure available and serves as a model for biochemical and structural analyses (9–11). ecCRP exists as a dimer with each protomer containing an N-terminal domain and a C-terminal domain. These two domains are linked by a long helix (C-helix) forming a hydrophobic dimerization interface. While the primary cAMP binding pocket (dissociation constant ( $K_d$ ) of about 27  $\mu\text{M}$ ) is located in the N-terminal domain, the C-terminal domain of ecCRP contains a helix-turn-helix motif responsible for DNA binding. Interestingly, a second cAMP binding site with much lower affinity ( $K_d \approx 2 \text{ mM}$ ) was observed between these two domains. It is worth noting that the primary cAMP binding pocket is far away from the helix-turn-helix motif, suggesting an allosteric regulation mechanism. The binding of cAMP results in rearrangements of C-helix (coil-to-helix transition), D-helix, and  $\beta 4-\beta 5$  loop of ecCRP, further reorientating the F-helix in a position optimal for DNA major groove binding. Biochemical and structural studies revealed that ecCRP can bind palindrome consensus sequences, which sharply kinks the DNA duplex to varying degrees (12, 13). It has also been proposed that the cAMP binding shifts the equilibrium of inactive CRP toward the active form, which explains the unusual cAMP binding affinity of CRP mutants (CRP\*) (11, 14). Interestingly, CRPs from some bacteria are not sensitive to cAMP binding; for example, the DNA binding affinity of *Mycobacterium tuberculosis* CRP (mtCRP) changes little upon cAMP binding (15, 16).

*Deinococcus radiodurans* is one of the important model organisms for studying the environmental adaptability mechanisms of bacteria. It can survive under extreme environmental stresses such as high-dose gamma radiation ( $D_{10}$  value of 10 kGy), DNA damage reagents (e.g., mitomycin C), and oxidative stress treatments, due to its super DNA damage repair ability and antioxidant capacity (17–19). However, how this radiation resistance evolved remains an open-ended question. One attractive theory is that *D. radiodurans* originated on Earth and specifically evolved super DNA damage repair ability in a long term drought environment. Its extreme ionizing radiation resistance is a by-product of adaptation to drought stress. Indeed, in addition to its super radiation-resistance, *D. radiodurans* can survive for a long-time during desiccation, which can also cause numerous DNA double-strand breaks in cells (similar to the biological effects of high-dose ionizing radiation). Transcriptome analysis further provides direct evidence for this hypothesis: a considerable part of the upregulated genes in response to drought and radiation stress in *D. radiodurans* overlap, and there is a palindromic consensus sequence in the promoter region of these genes, named radiation/desiccation response motif (RDRM) (20–22). These RDRM-containing genes are not only involved in the classical DNA repair processes (e.g., *recA* and *ssb*, which are also found in other bacteria) but also *Deinococcus*-specific genes with novel functions, such as some *ddr* (DNA damage response) series genes (23–25). Recent studies have uncovered an elegant RDRM regulation mechanism by a transcription factor protein DdrO and metalloprotease Pprl (26–28).

*D. radiodurans* contains four putative CRP family proteins, including DR0997 (also known as Ddrl), DR1646, DR2362, and DR0834. Among these candidates, Ddrl was identified as playing a major role in global regulation for the adaptation of *D. radiodurans* to various stresses (29, 30). *ddrl* was highly induced by gamma radiation treatments, and the inactivation of this gene sensitized cells to various stress environments including heat shock, radiation, DNA-damaging agents, and oxidation. Efforts to characterize the Ddrl binding sequence using electrophoretic mobility shift assay (EMSA) and *in silico* methods have led to the identification of hundreds of potential Ddrl target genes involved in divergent functions in metabolic pathways. Moreover, Ddrl was also shown to be involved in cell division, genome segregation, and plasmid maintenance (29). It

should be noted that *ddrl* does not belong to the RDRM gene group, and ecCRP only partially rescued the phenotype of the *ddrl* knockout strain.

In this work, we have determined the crystal structure of *D. radiodurans* Ddrl, which forms a dimer via coiled-coil interactions by fully folded C-helix of two neighboring protomers in the absence of cAMP. Together with the properly positioned HTH motif for binding to DNA, this Ddrl structure resembles the cAMP-activated CRP structure. Biochemical analysis suggested that Ddrl exhibited a very low affinity for cAMP binding. The addition of cAMP can, to a certain extent, decrease the affinity of Ddrl for target DNA. In contrast, Mn<sup>2+</sup> was able to enhance Ddrl binding to target DNA, especially sequences containing the RDRM-mimicking variant, indicating potential cross-talk between different transcription factors in *D. radiodurans* in response to environmental stress.

## RESULTS

### Overview of the Ddrl dimer structure

As noted in a previous study (30), *D. radiodurans* Ddrl contains 203 amino acids, which is 57 amino acids shorter than the original annotation. In addition to being conserved within Deinococcus species, Ddrl can be aligned with CRPs from other bacteria, sharing 52%, 29%, and 27% amino acid identities with its homologs from *Thermus thermophilus* (SdrP), *M. tuberculosis* (mtCRP), and *E. coli* (ecCRP), respectively (Fig. 1). Ddrl has a calculated isoelectric point of 5.30, which is similar to that of SdrP (5.43) but significantly lower than that of ecCRP (8.38) and that of mtCRP (9.57).

Full-length Ddrl containing a fused N-terminal 6 × His tag, an MBP-tag, and a TEV protease recognition sequence was expressed and purified. After tag removal during the purification steps, the untagged Ddrl was subjected to gel filtration chromatography to check its homogeneity and oligomeric properties. Unsurprisingly, Ddrl exists as a homodimer in solution (43.9 kDa, Fig. 2A). Ddrl crystals were grown and diffracted X-rays to 2.0 Å (Table S1). While the asymmetric unit contains one Ddrl monomer, two neighboring molecules form a dimer (Fig. 2B), consistent with its dimerization in solution (Fig. 2A). The final model, which comprises 7 α-helices and 12 β-strands, contains two domains: a nucleotide-binding N-terminal domain (NDB, residues 13–94) and a DNA-binding C-terminal domain (DBD, residues 122–202). These two domains are interconnected by a long linker α-helix (C-helix; residues 95–121). The NDB of Ddrl shares a canonical jelly roll topology with two layers of antiparallel β-strands, and DBD contains a winged HTH motif (E- and F-helices) critical for DNA binding (Fig. 2B and C). We performed a search with previously determined CRP structures in the PDB database (DALI server) using our Ddrl structure as the query, resulting in the closest structure of SdrP, the CRP family protein from *T. thermophilus* (PDB ID: 2ZCW), with root mean square deviation (RMSD) of 1.2 Å over 188 pairs of Ca atoms. As a member of the CRP family proteins, the Ddrl structure can also be aligned with other CRPs in their apo form, including ecCRP (PDB ID: 2WC2, RMSD value of 3.2 Å over 183 pairs of Ca atoms), and mtCRP (PDB ID: 3DOS, RMSD value of 2.1 Å over 189 pairs of Ca atoms).

Compared with ecCRP, the Ddrl structure exhibits variations in secondary structures (Fig. 1 and 2B). The very first N-terminal α-helix observed in ecCRP is disordered in the Ddrl structure. The α2 helix of Ddrl preceding the C-helix contains only three amino acids, which is much shorter than that of ecCRP (10 residues). An additional α-helix (α7) at the C-terminus of the DBD of Ddrl packs with the D-helix (Fig. 2C), which is not present in ecCRP. Importantly, the linker C-helix in the Ddrl structure is fully folded, in contrast to the partial folding of this region in ecCRP in the absence of cAMP (Fig. S1A and S1B; Fig. 2D) (31).

### The apo structure of Ddrl resembles the active CRP form

The coil-to-helix transition of the C-helix is the key structural feature distinguishing between active and inactive ecCRP structures (10, 11). Thus, the fully folded C-helix of apo Ddrl led us to suspect that our Ddrl without cAMP binding represents the active CRP

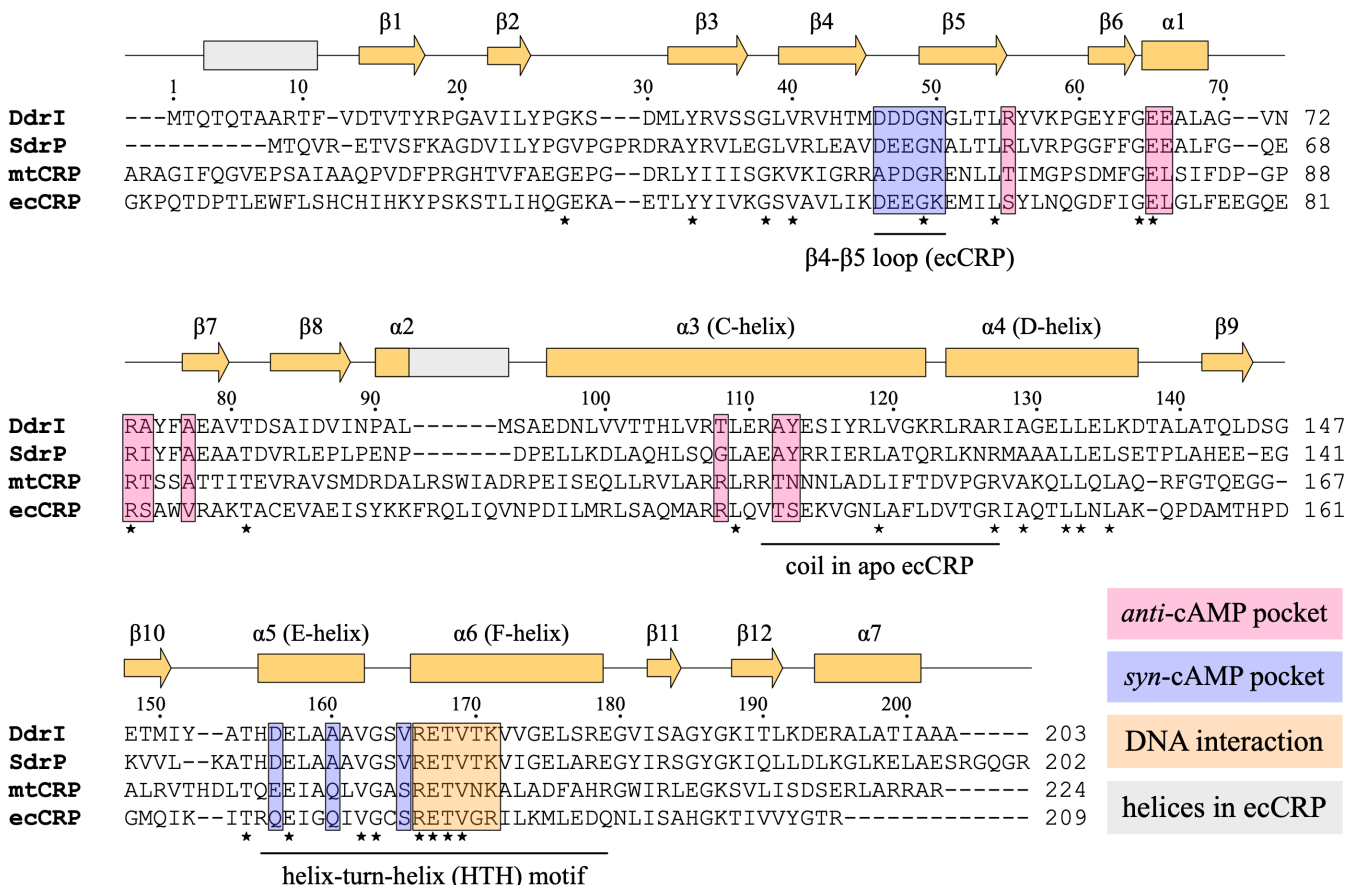


**FIG 1** Structure-based sequence alignment of CRPs from *Deinococcus radiodurans* (DdrI), *Thermus thermophilus* (SdrP), *Mycobacterium tuberculosis* CRP (mtCRP), and *Escherichia coli* (ecCRP). Secondary structures of DdrI (orange) and ecCRP (gray) are shown on top. Conserved residues are indicated by stars below the alignment. Residues involved in anti-cAMP binding pocket, syn-cAMP binding site, and DNA interactions are boxed and highlighted in distinct colors.

form. Indeed, the superposition of the DdrI dimer with the ecCRP-DNA-cAMP complex (PDB ID: 2CGP) results in an RMSD value of 2.1 Å over 181 pairs of Ca atoms (Fig. S1A). Despite the slight movement of solvent-exposed loops, two cAMP binding sites and the HTH motif of DdrI could align well with those in ecCRP-DNA-cAMP structure. Notably, compared with ecCRP apo structure lacking the cAMP, the β4-β5 loop and D-helix show noticeable movement, with the F-helix being in a position compatible with target DNA binding (Fig. 3A).

Given the good superimposition between DdrI and ecCRP-DNA-cAMP structure, target DNA containing TGTGA(N6)TCACA could easily be docked onto the HTH motif of DdrI (Fig. 3B). Previous studies have suggested that ecCRP protomer recognizes target DNA through interactions between the DNA half-site ( $T_1G_2T_3G_4A_5$ ) and the R<sub>180</sub>ETVGR<sub>185</sub> motif of the F-helix, and the same on the other side. These F-helix residues are important for DNA binding affinity and specificity of ecCRP (Fig. 3C). While Arg180 forms a hydrogen bond with the guanine base of G<sub>2</sub>, the G<sub>4</sub>:C<sub>4</sub> base pair is recognized by interactions between Arg185 and Glu181 with the guanine base (G<sub>4</sub>) and cytosine base (C<sub>4</sub>), respectively. Despite the conservation and similar rotamer states of the first four amino acids (R<sub>166</sub>ETV<sub>169</sub>), the last two amino acids of the DdrI F-helix, Thr170 and Lys171 (equivalent to Gly184 and Arg185 in ecCRP), are not conserved (Fig. 1 and 3C).

EMSA using different lengths of target DNA containing TGTGA(N6)TCACA was performed to further confirm the DNA binding affinity of DdrI in the absence of cAMP (Fig. 3D). DdrI was able to form a stable complex with target DNA in a length-dependent manner: target DNA of 26 bp constituted a length threshold, below which no stable complex was detected (Fig. 3D). The DNA binding affinity constant of DdrI was measured

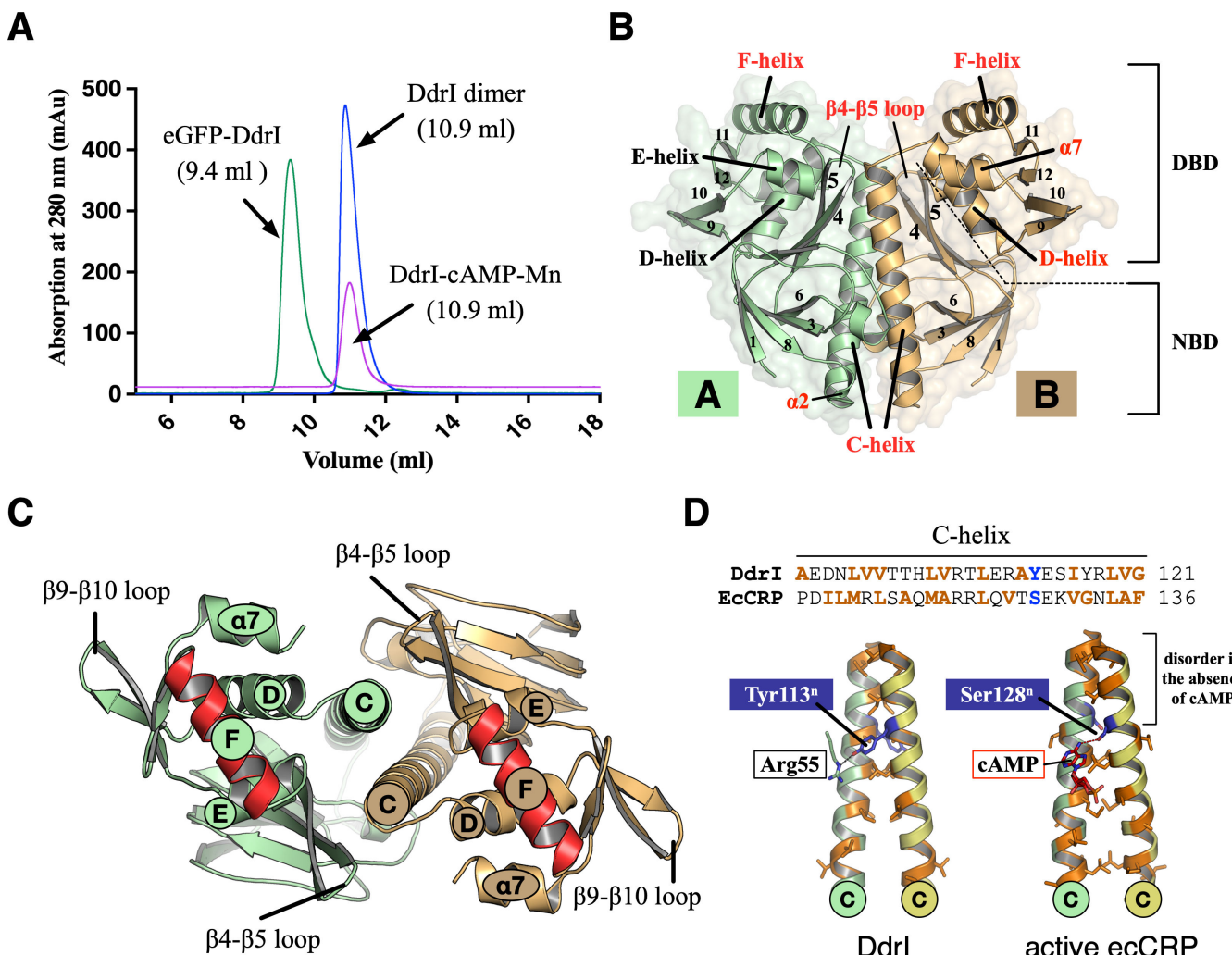
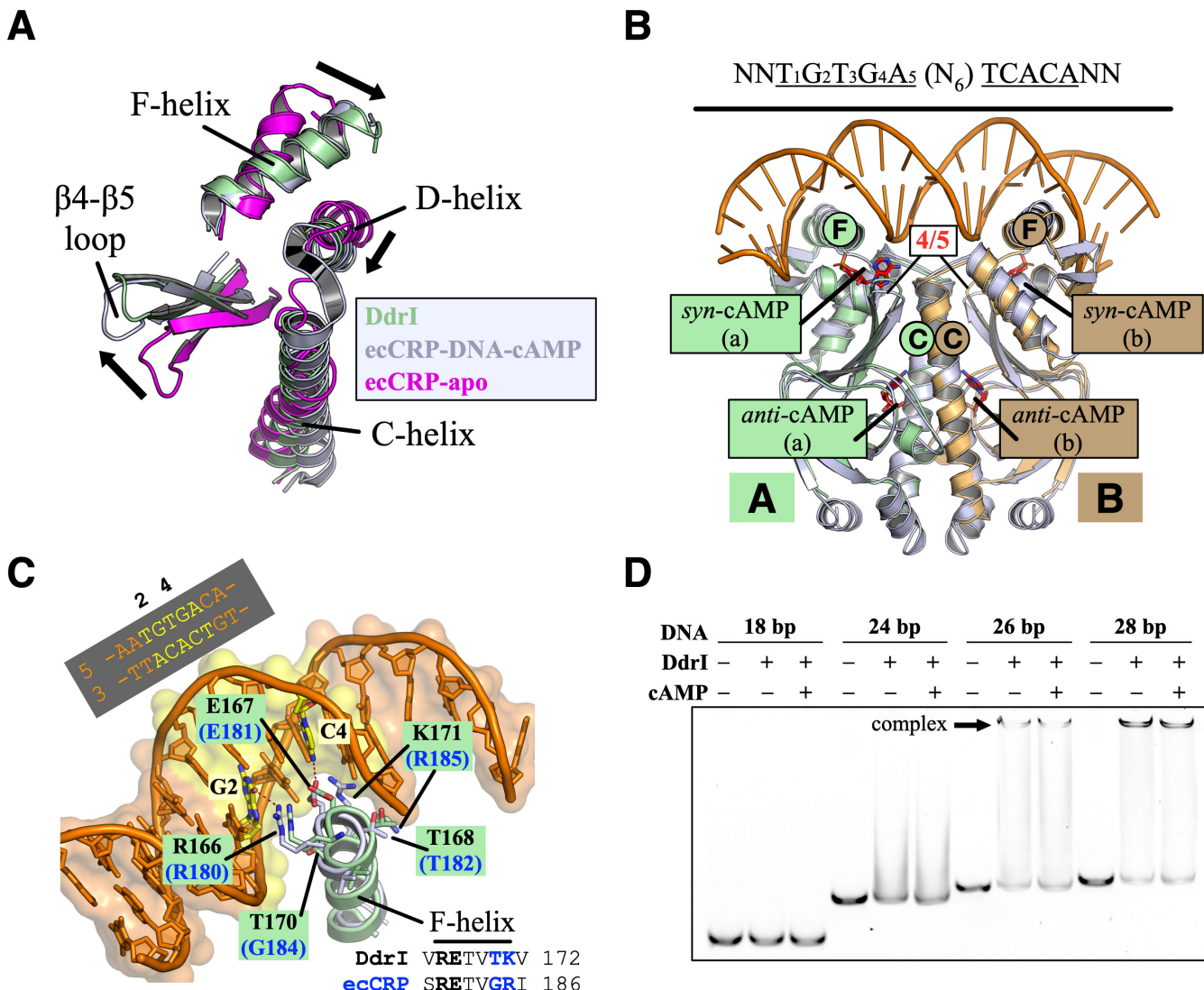


**FIG 2** Overview of the Ddrl dimer structure. (A) Size-exclusion chromatography demonstrates the presence of dimeric Ddrl and eGFP-Ddrl. The addition of cAMP and Mn<sup>2+</sup> (Ddrl-cAMP-Mn) did not affect its dimer formation. (B) Side view of the overall structure of Ddrl. The Ddrl dimer is depicted in cartoon representation, with two protomers colored green (A) and wheat (B), respectively. The  $\alpha$ -helices,  $\beta$ -strands, nucleotide-binding N-terminal domain (NBD), and DNA-binding C-terminal domain (DBD) of each protomer are labeled. (C) Top view of the overall structure of the Ddrl dimer. Functionally important  $\alpha$ -helices and loops are labeled, with the F-helix highlighted in red. (D) The C-helices involved in CRP dimerization. The amino acid sequence is shown on top, with hydrophobic residues in orange. cAMP (shown in red) and the hydrophobic residues (orange sticks) are displayed, with Tyr113 (Ddrl) and Ser128 (ecCRP) highlighted in blue.

by microscale thermophoresis (MST) analysis. Target DNA (28 bp) was labeled with 5'-Cy5 and kept at a constant concentration of 20 nM in MST buffer at 30°C, followed by Ddrl titration from 0.305 nM to 10 μM. Fitting the data according to the  $K_d$  Fit Model resulted in a dissociation constant of  $K_d = 225.9 \pm 35.5$  nM (Fig. 4A; Table 1). These results indicate that Ddrl can form an active dimer in the absence of cAMP molecules, which is consistent with structural observations (Fig. 3A and B).

## The discrepancies in the high-affinity cAMP (*anti*-cAMP) binding pocket

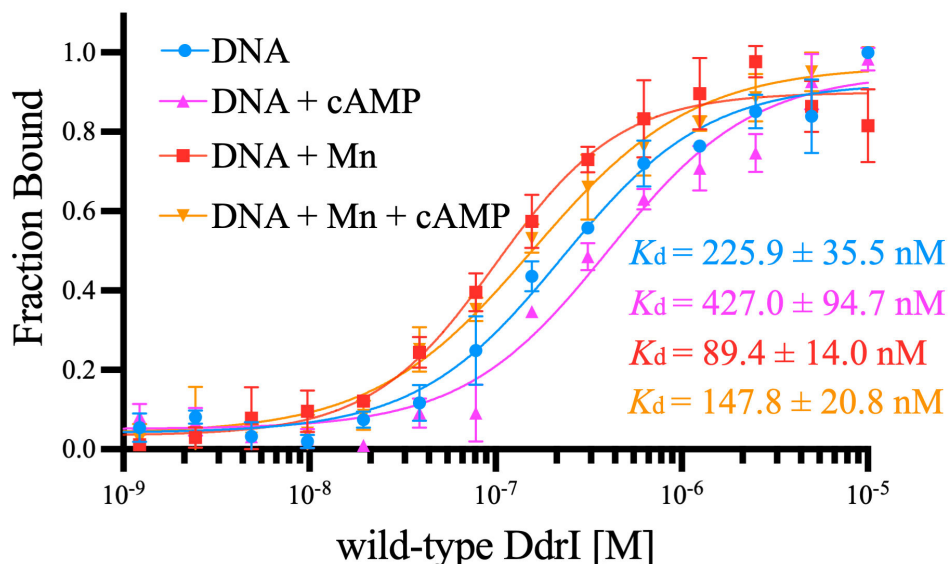
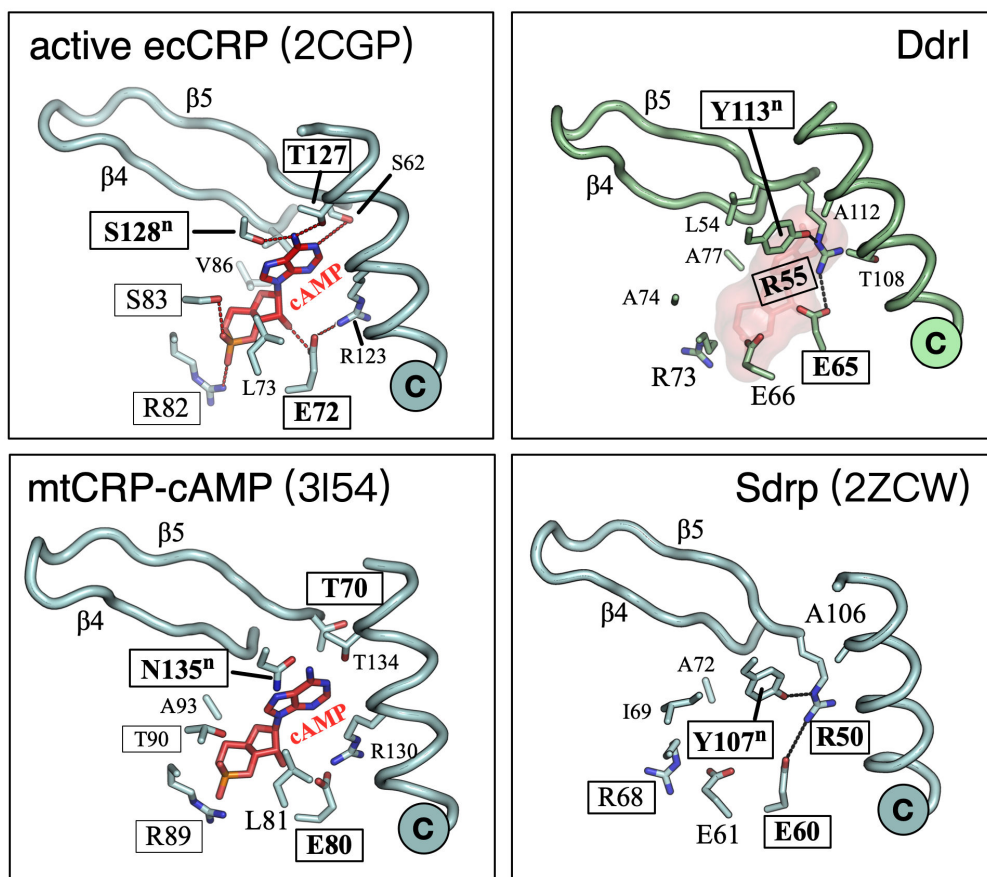
The primary cAMP binding site is close to the coiled-coil dimerization interface formed by two neighboring C-helices (Fig. 3B). In the absence of cAMP, the C-terminal portion of the C-helix of apo ecCRP is unstructured (as loop region), interacting with the  $\beta$ 4- $\beta$ 5 loop of the neighboring protomer (Fig. S1A). Upon the cAMP accommodation,  $\beta$ 4 and  $\beta$ 5 exhibit noticeable movement, resulting in the  $\beta$ 4- $\beta$ 5 loop shifting toward the DBD (Fig. 3A). In addition, the C-helix directly interacts with the cAMP, undergoing a substantial coil-to-helix transition to be fully folded into a long  $\alpha$ -helix. Not surprisingly, this cAMP



**FIG 3** Apo Ddrl structure resembles the active CRP form. (A) Superposition of the secondary elements critical for allosteric transition of CRP. The structures of Ddrl (from this study), apo ecCRP (PDB ID: 2WC2), and ecCRP-DNA-cAMP (PDB ID: 2CGP) are colored green, magenta, and gray, respectively. The black arrowheads indicate the shifts in the C-helix (coil-to-helix transition), D-helix, F-helix, and β4-β5 loop that occur during the activation of ecCRP by cAMP. (B) Superposition of the Ddrl dimer (colored as in Fig. 2B) with the ecCRP-DNA-cAMP complex (gray). Two cAMP binding sites from each protomer are labeled, with the cAMP molecules shown as red sticks. The C-helix, F-helix, and β4-β5 loop (4/5) are labeled. (C) The zoom-in view of the F-helices of Ddrl (green) and ecCRP-DNA-cAMP (gray), with the palindrome consensus sequence indicated above. The F-helix residues of Ddrl (labeled in black) and ecCRP (labeled in blue) are shown as sticks. The half-site of the palindrome consensus sequence is highlighted in yellow, with G<sub>2</sub> and C<sub>4</sub> labeled. The red dashed lines indicate the interactions between protein and DNA. (D) EMSA shows the DNA binding capability of Ddrl. 5'-Cy5-labeled target DNA containing the palindrome consensus sequence (100 nM, with lengths of 18–28 bp) was incubated with 1 μM Ddrl protein in the absence or presence of 100 μM cAMP at 30°C for 30 min. Black arrowheads indicate the stable complexes.

binding pocket of Ddrl appears to be well structured in terms of the arrangement of surrounding secondary structure elements (Fig. 3B and 4B).

There are discrepancies concerning the cAMP interacting residues based on structural-based sequence alignment (Fig. 1 and 4B). cAMP is bound in the *anti*-conformation in classic CRP complexes (e.g., ecCRP and mtCRP) through several key residues (Fig. 4B). In active ecCRP (PDB ID: 2CGP), the phosphoribose of cAMP is held in place by Glu72, Leu73, Arg82, Ser83, and Val86; the adenine base interacts with Ser62, Thr127, and Ser128<sup>n</sup> (n: from the neighboring protomer). In addition, Arg123 forms a salt bridge with Glu72, which is important for cAMP discrimination. Among these

**A****B**

**FIG 4** DNA binding affinity and the *anti-cAMP* binding site of DdrI. (A) Target DNA binding affinities determined by MST. Target DNA (28 bp) was labeled with 5'-Cy5 and maintained at a constant concentration of 20 nM in MST buffer at 30°C. This was followed by the titration of wild-type DdrI, ranging from 0.305 nM to 10 μM. If necessary, 10 μM Mn<sup>2+</sup> and 100 μM (Continued on next page)

**FIG 4 (Continued)**

cAMP were added. Binding curves represent the change in normalized fluorescence (Fraction Bound), and the  $K_d$  values were calculated using the  $K_d$  Fit Model. (B) The high-affinity cAMP (*anti*-cAMP) binding pocket of CRPs from ecCRP (PDB ID: 2CGP), Ddrl (this study), mtCRP (PDB ID: 3I54), and SdrP (PDB ID: 2ZCW). The C-helix,  $\beta$ 4, and  $\beta$ 5 are shown as ribbons and labeled. The *anti*-cAMP and cAMP-interacting residues are shown as sticks and labeled. Residues equivalent to the TS motif (Thr127-Ser128), RS motif (Arg82-Ser83), and Glu72 of ecCRP are boxed. The dashed lines indicate the interactions between residues and cAMP within this binding pocket.

phosphoribose-interacting residues, Ddrl has two conserved residues, Glu65 and Arg73 (equivalent to ecCRP Glu72 and Arg82) but three substitutions: Glu66, Ala74, and Ala77 (equivalent to ecCRP Leu73, Ser83, and Val86, respectively) (Fig. 1 and 4B). Notably, all the residues interacting with the adenine base are not conserved compared with ecCRP or mtCRP; they are replaced by Arg55, Thr108, Ala112, and Tyr113<sup>n</sup> (equivalent to ecCRP Ser62, Arg123, Thr127, and Ser128<sup>n</sup>, respectively).

In contrast to the cavity occupied by the cAMP molecule in ecCRP, this binding pocket of Ddrl is partially filled with Tyr113<sup>n</sup>-Arg55-Glu65 (equivalent to ecCRP Ser128<sup>n</sup>, Ser62, and Glu72) (Fig. 4B). Instead of interacting with the adenine base as its ecCRP equivalent does, Arg55 of Ddrl forms hydrogen bonds with both Tyr113<sup>n</sup> and Glu65, leading to insufficient space for cAMP accommodation. Moreover, Tyr113<sup>n</sup> packs behind a leucine residue. This residue, Leu54, is conserved within CRPs, which participates in the dimerization interface formation through hydrophobic interactions in both Ddrl and ecCRP structures. The addition of cAMP (100  $\mu$ M) slightly decreased the DNA binding affinity of Ddrl (Fig. 4A, DNA + cAMP). Thereby, putative cAMP binding to this site should be excluded.

### The second cAMP (*syn*-cAMP) binding site

The second cAMP molecule is bound in the *syn* conformation. This was first observed in the ecCRP-DNA structure in the presence of 2 mM cAMP during the crystallization (12). In contrast to the buried cAMP in the first binding pocket, this cAMP binding site is solvent-exposed. Given that this *syn*-cAMP is located between the DBD and NTD domains and interacts with the  $\beta$ 4- $\beta$ 5 loop, HTH motif, neighboring C-helix, and DNA (Fig. 3B; Fig. S1A), it has been proposed to be involved in the activation of ecCRP by cAMP. The putative binding site of this *syn*-cAMP is also solvent-accessible in the Ddrl structure.

As a hydrophobic molecule, the adenosine of *syn*-cAMP in ecCRP-DNA complex packs against the C-terminus of the  $\beta$ 4- $\beta$ 5 loop (Lys57-Glu58-Met59), Gln170, and Gln174, with the phosphate oxygen interacting with Arg180 (main chain) and Glu181 (a water-mediated interaction) (Fig. 5). The latter two amino acids are critical for the DNA binding of CRPs, interacting with the G-C base pairs at positions 2 and 4 of the target sequence (Fig. 3C). However, residues packing the putative *syn*-cAMP show deviations in Ddrl, with Asn50-Gly51-Leu52, Asp156, and Ala160 in the corresponding positions (Fig. 5).

**TABLE 1** DNA binding affinities determined by MST

DNA	Protein	Mn <sup>2+</sup>	cAMP	$K_d$ (nM)
Target DNA	WT	—	—	225.9 ± 35.5
		—	+	427.0 ± 94.7
		+	—	89.4 ± 14.0
		+	+	147.8 ± 20.8
D156Q	WT	—	—	45.9 ± 8.5
		—	+	32.7 ± 7.7
		+	—	22.7 ± 3.4
		+	+	24.4 ± 4.6
<i>ddrB</i> -mimic	WT	—	—	No binding
		+	—	20.3 ± 6.4 $\mu$ M

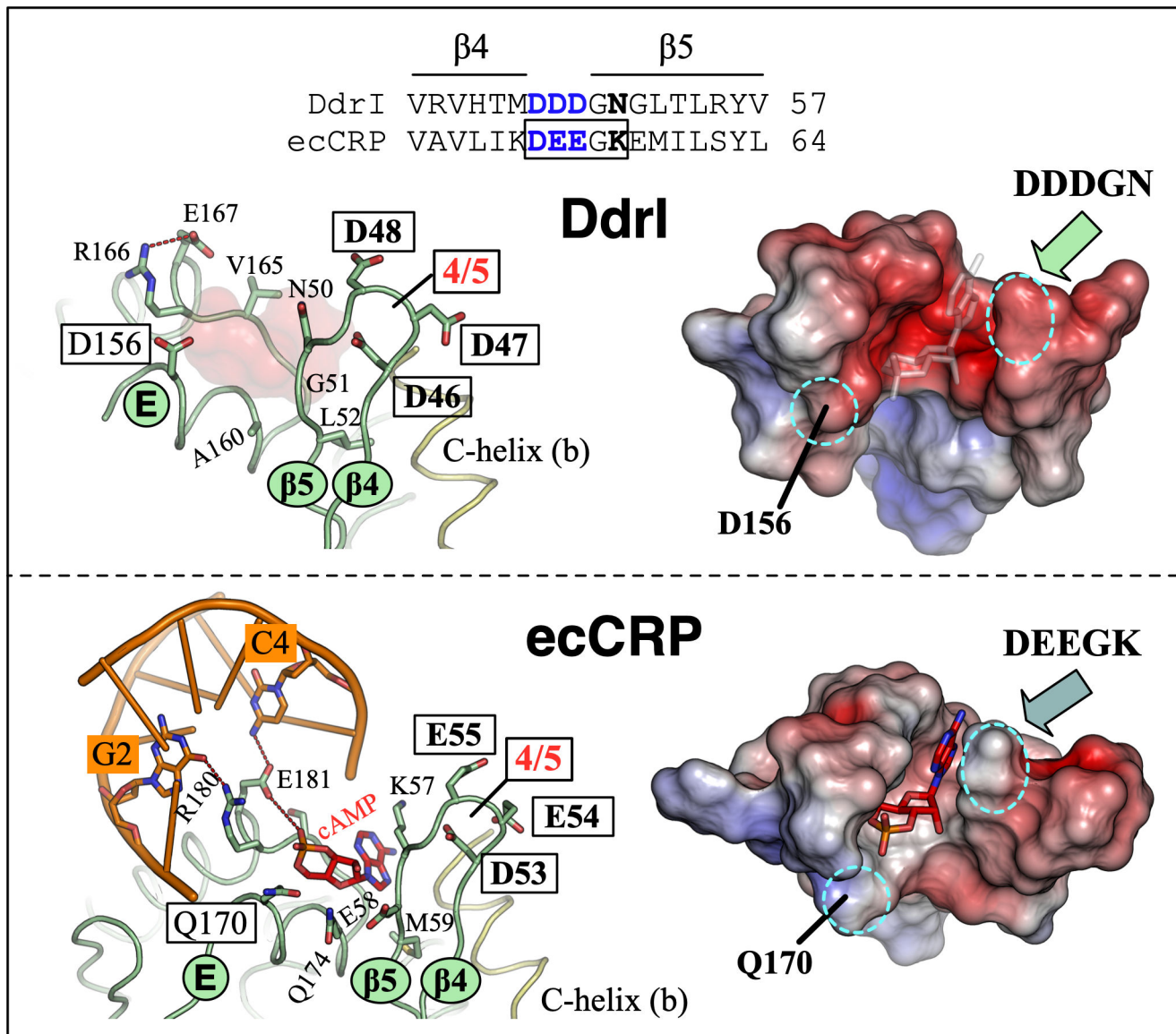


**FIG 5** The second cAMP (*syn*-cAMP) binding site. Helices,  $\beta$ -strands, and  $\beta$ 4– $\beta$ 5 loop (labeled 4/5) of Ddrl (top) and ecCRP (PDB ID: 2CGP, bottom) are shown in ribbon representation with labels. Residues and *syn*-cAMP are depicted as sticks, colored green and red, respectively. The electrostatic potential of the *syn*-cAMP binding surface was determined using the APBS and is shown as a solvent-excluded surface. Blue and red denote positive and negative charge potentials, respectively, on a scale of  $\pm 7\text{kT}_\text{e}^{-1}$ . Dashed lines highlight interactions between residues and *syn*-cAMP within this binding pocket.

Interestingly, variations of these  $\beta$ 4– $\beta$ 5 loop residues lead to  $\beta$ -strand formation in this region, resulting in an elongated (two amino-acids longer)  $\beta$ 5 strand compared with that of ecCRP. Moreover, the  $\beta$ 4– $\beta$ 5 loop before these packing residues comprises triple-aspartate (Asp46-Asp47-Asp48) different from its equivalent in ecCRP (Asp46-Glu47-Glu48). Analysis of the distribution of the electrostatic surface potential suggested that this putative cAMP binding site, in addition to the  $\beta$ 4– $\beta$ 5 loop, is more negatively charged in Ddrl than in ecCRP (Fig. 5).

Given the different local environment of the *syn*-cAMP binding site of Ddrl, we checked the cAMP binding affinity by MST analysis (Fig. 6A). Ddrl was expressed containing an N-terminal fused eGFP and kept at a constant concentration of 20 nM in MST buffer at 30°C. This was followed by cAMP titration from the nanomolar to the millimolar range. Low concentrations of cAMP (76.3 nM to 313.0  $\mu\text{M}$ ), corresponding to the concentrations used for high-affinity cAMP binding constants measurements of

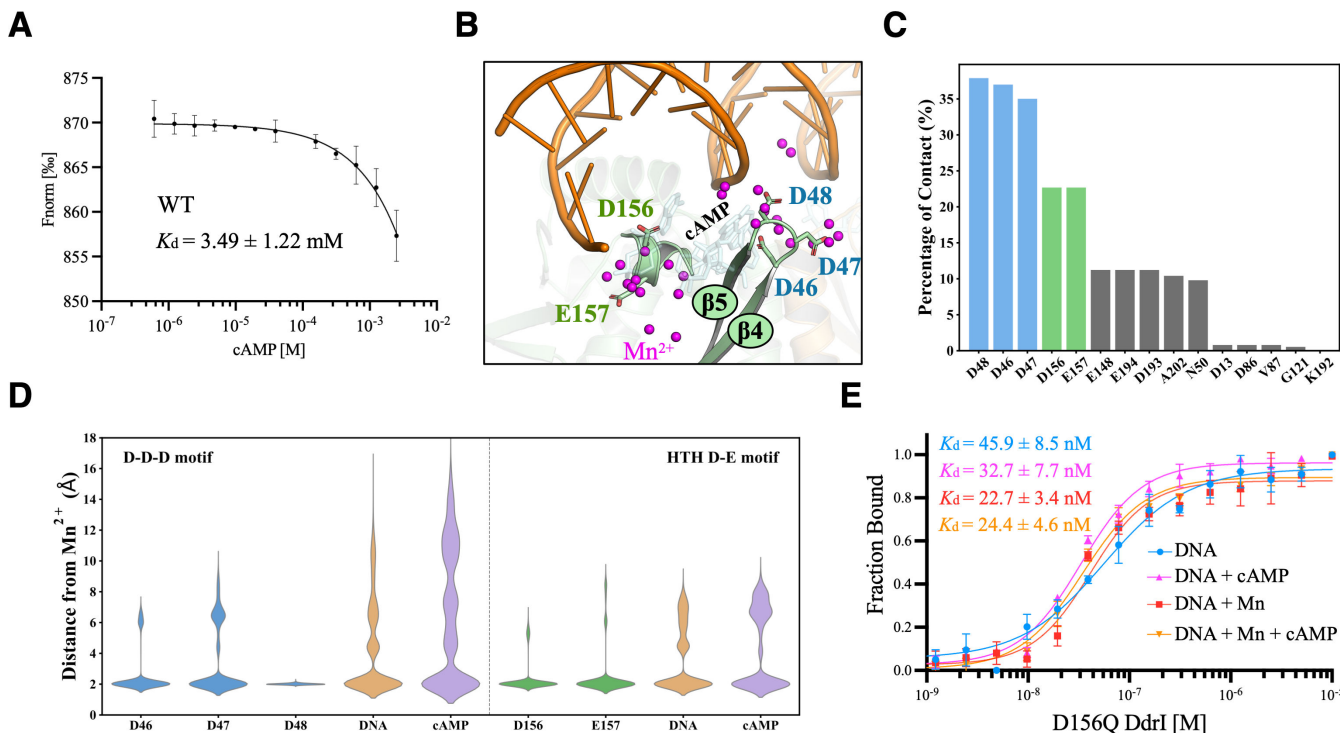


**FIG 6** Molecular dynamics simulations reveal that Mn<sup>2+</sup> mediates the interaction between Ddrl and the RDRM-mimicking DNA. (A) The cAMP binding constant of wild-type Ddrl. N-terminal fused eGFP-Ddrl was kept at a constant concentration of 20 nM, followed by cAMP titration. Binding curves represent the change in normalized fluorescence (Fnorm[%]), and the  $K_d$  values were calculated using the  $K_d$  Fit Model. (B) Molecular dynamics simulations of Mn<sup>2+</sup> binding to Ddrl in the presence of RDRM-mimicking DNA and cAMP. The E-helix, β4, and β5 strands are shown in cartoon representation with labels. Residues involved in two hotspots and Mn<sup>2+</sup> are colored blue (Asp46-Asp47-Asp48), green (Asp156-Glu157), and magenta, respectively. (C) The percentage of contact with Mn<sup>2+</sup> of all protein residues indicates predominant Mn<sup>2+</sup> hotspots: Asp46-Asp47-Asp48 (blue) and Asp156-Glu157 (green). (D) Distribution of distances between Mn<sup>2+</sup> and coordinating atoms on hotspot residues, DNA, and cAMP. (E) DNA binding affinities of D156Q mutant Ddrl. Target DNA (28 bp) was labeled with 5'-Cy5 and maintained at a constant concentration of 20 nM in MST buffer at 30°C. This was followed by titration of D156Q mutant protein, ranging from 0.305 nM to 10 μM. If necessary, 10 μM Mn<sup>2+</sup> and 100 μM cAMP were added. Binding curves represent the change in normalized fluorescence (Fraction Bound), and the  $K_d$  values were calculated using the  $K_d$  Fit Model.

classical CRPs, showed no ligand binding. This was consistent with the EMSA assay and structural observations of the invalid anti-cAMP binding pocket of Ddrl (Fig. 3D and 4B). Fitting the data according to the  $K_d$  Fit Model results in a dissociation constant of  $K_d = 3.49 \pm 1.22 \text{ mM}$  (Fig. 6A), a value in a range commensurate with syn-cAMP binding affinity of other CRPs (12).

### Enhancement of target DNA binding by Mn<sup>2+</sup>

Transcriptional regulation of gene expression at targets containing the RDRM motif is critical for the adaptation of *D. radiodurans* in response to environmental stresses (22). Based on the partial overlaps of the consensus sequences between Ddrl regulons and the RDRM motif, it was hypothesized that Ddrl may also play a regulatory role for some radiation/desiccation response (RDR) genes (29). Variant sequences containing a portion of RDRM (TGTAA, present in the RDRM sequences of *ddrB* and *ddrC*) were investigated for Ddrl binding (Fig. S2). These variants contain a T-A base mutation at the G<sub>4</sub>:C<sub>4</sub> position and various substitutions on the other half of DNA. Unlike the high-affinity binding of target DNA (Fig. 3D and 4A), Ddrl was unable to bind these two variants under the same experimental conditions *in vitro*: no protein-DNA complex formation was observed by EMSA (Fig. S2A), and no binding signal of *ddrB*-mimic was detected by MST analysis (Fig. S2B).

*D. radiodurans* has an unusually high intracellular Mn concentration (millimolar), which can activate RDR gene expression through specific cleavage of DdrO by Pprl protease (26, 27). Given that the *syn*-cAMP binding site of Ddrl, which is close to the DNA binding surface, is more negatively charged (Fig. 5A), we were curious whether Mn also plays a role in Ddrl regulation. The reactions containing Mn<sup>2+</sup> resulted in dissociation constants of  $K_d = 89.4 \pm 14.0$  nM, which was approximately 2.5-fold lower than that without Mn<sup>2+</sup> (Fig. 4A; Table 1). Interestingly, despite no stable complex being observed by EMSA assays, Ddrl exhibited weak DNA binding capability to the *ddrB*-mimicking sequence ( $K_d = 20.3 \pm 6.4$  μM) in the presence of Mn<sup>2+</sup> (Fig. S2B), which was two orders of magnitude higher than that of the target DNA. Interestingly, cAMP (100 μM) appeared to play a negative role in Ddrl binding to DNA, resulting in approximate 1.9- and 1.6-fold increases in  $K_d$  values for target DNA binding in the absence and presence of Mn<sup>2+</sup>, respectively (Fig. 4A; Table 1).

Molecular dynamics simulations were performed to further investigate the possible role of Mn<sup>2+</sup> involved in RDRM-mimicking DNA binding of Ddrl. In the presence of Mn<sup>2+</sup>, cAMP appears to exhibit large fluctuation in the *syn*-cAMP binding site, partly exiting the vicinity of the β4 and β5 loops from time to time (Fig. 6B). Notably, Mn<sup>2+</sup> predominantly congregates at two critical binding hotspots: (i) coordinated by Asp46, Asp47, and Asp48 of the β4-β5 loop; (ii) interacting with Asp156 and Glu157 (Fig. 6B and C). Interestingly, the findings in these two regions are consistent with the negative electrostatic potentials of the Ddrl (Fig. 5). We next performed a second round of simulations to check the interactions between Mn<sup>2+</sup> and surrounding residues. Mn<sup>2+</sup> exhibits high specificity and stability to these residues, especially Asp48 and Asp156 (Fig. 6D). Moreover, in most replicas, the backbone phosphates of DNA and the cAMP are also involved in Mn<sup>2+</sup> coordination (Fig. 6D); Mn<sup>2+</sup> specifically neutralizes the negatively charged DNA-interacting interface of Ddrl (Fig. 6B), facilitating more robust interactions between Ddrl and DNA, thereby enhancing Ddrl binding to the RDRM-mimicking DNA.

Asp156 was mutated to electrically neutral glutamine residue (D156Q, as its ecCRP equivalent) to measure its DNA binding affinities (Fig. 6E; Table 1). While the DNA binding constant for the D156Q mutant was  $K_d = 45.9 \pm 8.5$  nM, the addition of Mn<sup>2+</sup> or Mn<sup>2+</sup>-cAMP resulted in increased target DNA binding ( $K_d = 22.7 \pm 3.4$  nM and  $K_d = 24.4 \pm 4.6$  nM, respectively). Moreover, cAMP was able to enhance the D156Q binding activity ( $K_d = 32.7 \pm 7.7$  nM). These numbers were approximately 10-fold lower than that of the wild-type Ddrl, which are comparable to previous biochemical studies of activated mtCRP (15).

## DISCUSSION

Since the discovery of the very first CRP in *E. coli* more than five decades ago, the question of how transcription factors sense environmental stresses and transmit the signal for altered DNA binding has attracted increasing attention. Although the evolution of *D. radiodurans* is not fully understood, this bacterium is uniquely suited for studying bacterial adaptation to environmental stresses because of its cellular robustness. Several transcription factors have been characterized, which are critical for its growth and survival during stress conditions. Transcription factors including OxrR and PerR are important for the antioxidation of *D. radiodurans*, while DtxR and Mur appear to be involved in maintaining intracellular metal ion homeostasis (32, 33). It is worth noting that the exceptionally high intracellular Mn concentration (mM range) correlates with the extreme radio-resistance of this bacterium (34). Recent studies revealed sophisticated regulation of RDRM genes. Derepression of transcription factor DdrO bound to promoters could be activated by physical interactions between the corresponding Pprl protease and single-stranded DNA (26).

The overall structure of Ddrl without cAMP resembles an activated CRP-cAMP conformation, similar to active ecCRP-cAMP and mtCRP-cAMP structures. According to 16S rRNA sequences, *D. radiodurans* and *T. thermophilus* belong to the same phylum (the *Deinococcus-Thermus* phylum); therefore, it is not surprising that Ddrl showed

the highest structural similarity with SdrP, a CRP family protein characterized in *T. thermophilus*. Indeed, stress-related proteins of *Deinococcales* usually share structural commonalities in some ways with their *Thermales* homologs, which were frequently used as the starting search model during the structure determinations of *Deinococcus* proteins (35–37). Interestingly, SdrP was speculated to be active independent of any effector molecule including the cAMP (38). Given the distinct evolution of *Deinococcus-Thermus*, CRP family proteins from this phylum may have evolved differently from those of cAMP-dependent CRPs (e.g., ecCRP). This could also be due to different physiological and metabolic properties between *D. radiodurans* and *E. coli*, which correlated with the partial compensation for the *ddrl*-knockout phenotype by ecCRP (29). In contrast to the preferential utilization of glucose over other carbon sources in *E. coli*, *D. radiodurans* uses amino acids as the primary energy source, with fructose, pyruvate, and lactate being preferred over glucose (39). In addition, classic adenylate cyclase responsible for cAMP synthesis has not been characterized in *D. radiodurans*, although an altered cAMP concentration after radiation has been reported (40).

Ddrl appears to use an alternative strategy that does not require cAMP binding (Fig. 4). Given the amphiphilic behavior of both Tyr113<sup>n</sup> and adenine, residue interactions (Tyr113<sup>n</sup>-Arg55-Glu65) evolved in Ddrl *per se* effectively mimic the cAMP binding, which is consistent with its DNA binding capability in the absence of cAMP (Fig. 3D and 4A). This is also consistent with the amino acid composition for C-helices dimerization (Fig. 1 and 2D). The C-helix of ecCRP comprises repeated hydrophobic residues except at the position of Thr127-Ser128<sup>n</sup> (the TS motif). The binding of cAMP to ecCRP brings the two C-helices closer together, overcoming the interruption at the TS position and resulting in a coil-to-helix transition after the TS motif. However, in Ddrl, the equivalent residue (Tyr113<sup>n</sup>) is anchored by Arg55, leading to an intrinsically fully folded C-helix. Indeed, hydrophobic substitutions at the TS motif (CRP\* mutants) result in high CRP activities even in the absence of cAMP (41). A second factor contributing to the activated Ddrl dimer without cAMP may be the varying secondary elements around the C-helix. Compared with ecCRP, Ddrl has a shortened  $\alpha$ 2 helix before the C-helix and an elongated  $\beta$ 5 strand interacting with the C-terminus of the C-helix (Fig. 2B). Furthermore, Ddrl contains an additional  $\alpha$ 7 helix packed behind the D-helix (Fig. 2C). According to nuclear magnetic resonance (NMR) analysis, the D-helix undergoes a remarkable motion to form extensive interactions with the C-helix during the cAMP-mediated allosteric transition (31). Thus, these interactions may enhance the coiled-coil dimer interface formed by two C-helices, which facilitate the overall conformation of Ddrl in its active CRP form.

Given the energy-unfavored *syn*-conformation and significantly lower CRP-binding affinity in the millimolar range, whether the second cAMP binding site exists under physiological conditions remains enigmatic. Nevertheless, given its location (between the DBD and NTD) and cAMP interactions with both protein (HTH motif and  $\beta$ 4- $\beta$ 5 loop) and DNA, the *syn*-cAMP binding site is believed to play a biological role in the regulation of CRP activities. In the case of Ddrl, all the residues, except Glu167, involved in *syn*-cAMP-ecCRP interactions are not conserved. Interestingly, among these varied *syn*-cAMP-interacting residues, high-frequency mutations at Gln170 of ecCRP (equivalent to Asp156 of Ddrl) were observed in evolution experiments under a cAMP-deficient background (42). Moreover, Ddrl possesses a much lower calculated isoelectric point and more negatively charged *syn*-cAMP binding site compared to those of ecCRP, featuring an altered triple-aspartate motif in the  $\beta$ 4- $\beta$ 5 loop (Fig. 5). Despite their chemical similarity, previous studies have hinted at functional disparities between aspartates and glutamates. Compared with glutamate, aspartate exhibits higher conservation and frequently functions as a helix N-capping residue (43, 44), thereby accounting for the elongated  $\beta$ 5 strand observed in Ddrl (Fig. 5). Furthermore, aspartate demonstrates a proclivity to form more stable complexes with divalent cations, including Mn<sup>2+</sup>, in solution than glutamate (45). Considering the exceptionally elevated intracellular Mn concentration in *D. radiodurans*, it is unsurprising that Mn<sup>2+</sup> proved capable of augmenting the DNA binding affinity of Ddrl (Table 1). This enhancement may facilitate either transient or

stable protein-DNA interactions by mitigating the negative charge repulsions between the *syn*-cAMP binding site and the DNA phosphate backbone (Fig. 6B). Indeed, the presence of Mn<sup>2+</sup> is frequently documented in the structures of *Deinococcus* proteins, playing a pivotal role in enzymatic catalysis and protein folding (46, 47). As an illustration, an Mn ion is positioned at the dimer interface of the *D. radiodurans* RNase J protein, modulating its dual activity during RNA cleavage (48).

Ddrl was able to form a stable complex with consensus CRP target DNA (Fig. 3D), which is consistent with previous structural, genetic, and *in silico* studies (10, 11). On the other hand, Ddrl also interacted with a variant of this sequence containing an RDRM-mimic in the presence of Mn<sup>2+</sup>, but with a much lower binding affinity *in vitro* (Fig. S2B). Together with the increased intracellular DdrB protein (RDRM regulon) in the *ddrl* knockout strain and the partial overlap between the putative Ddrl binding sequence and RDRM, our results further confirmed potential cross-talk between Ddrl and DdrO. Other factors may also contribute to such cross-talk that one RDRM could be regulated by these two transcription factors: (i) Two residues equivalent to Gly184 and Arg185 of ecCRP are not strictly conserved across different CRPs. In contrast to the unchanged activity upon conservative substitution of R185K, Gly184 is important for both DNA binding and RNA polymerase (RNAP) recruitment by ecCRP (49). Therefore, variations in these two residues in Ddrl may have an impact on RNAP interacting with RDRM. (ii) Interactions between activating regions of CRP and RNAP are required for its cellular function. Our Ddrl structure superimposed well onto TAP (another CRP homolog in *T. thermophilus*) in the intact bacterial class II transcription activation complex (PDB ID: 5I2D) (50). TAP also contains an additional helix equivalent to  $\alpha$ 7 of Ddrl, which interacts with the RNAP  $\alpha$  subunit C-terminal domain. Notably, cAMP was not required for this complex formation, which confirms the active conformation of Ddrl solved in the current study. Given the interactions between  $\alpha$ 7 and the D-helix, this may explain a prerecruitment mechanism that differs from ecCRP recruitment (51); CRPs with an additional helix may bind to RNAP prior to DNA. Moreover, the mechanism of RNAP recruitment after DdrO cleavage remains unclear. Based on the possible RDRM binding and RNAP interaction of Ddrl, Ddrl may function as a mediator for RDRM activation after DNA damage. (iii) Given the low binding affinity of *syn*-cAMP, other effector molecules, such as cGMP, could also be involved in Ddrl regulation. It should be noted that the *relA* function is normal in *D. radiodurans*, and it is induced under growth conditions with limited amino acids (52), the most preferred carbon source for this organism. Thus, ppGpp synthesized by RelA is also a candidate Ddrl effector. (iv) Single-molecule analyses have revealed cooperative binding of transcription factors to DNA, which is highly dynamic (53). The highly condensed genome of *D. radiodurans* is expected to contribute to its robustness with less damage from environmental stresses. Factors such as local DNA structures or cooperative/competitive binding between multiple transcription factors may also regulate RDRM gene expression.

To adapt to their environment, bacteria have evolved diverse transcription factors that participate in the global regulation of gene expression. On the other hand, the same transcription factors in different bacteria have also evolved to help them adapt to specific environments according to their characteristics. The Ddrl protein in this study is one example, exhibiting different structural and biochemical properties from classical CRPs. Given that the characteristics of ecCRP are likely to have evolved from a simple DNA-binding protein with limited specificity (54), elucidating the cAMP-independent regulatory mechanism of this protein and its possible cross-talk with other transcription factors, such as DdrO, would provide valuable information for better understanding the environmental adaptability of the extreme microorganism *D. radiodurans*.

## MATERIALS AND METHODS

### Bacterial strains, plasmids, and growth conditions

*D. radiodurans* strains (ATCC 13939) were grown at 30°C in TGY broth (0.5% tryptone, 0.3% yeast extract, and 0.1% glucose) or on TGY plates with 1.5% (wt/vol) agar powder. *E. coli* strains were cultivated in LB broth (1% tryptone, 0.5% yeast extract, and 1% NaCl) or on LB plates with 1.5% (wt/vol) agar at 37°C. The full-length *ddrl* gene (DR0997, GenBank accession number A2G07\_08515) was amplified by PCR from *D. radiodurans* genomic DNA and cloned into the NdeI and BamHI sites of the pET28-HMT vector (26). Site-directed mutation of the Ddrl sequence (D156Q) was generated using a QuickChange site-directed mutagenesis kit (Stratagene) as previously described (37). All the strains and plasmids are listed in Table S2. All the primers and DNA substrates are listed in Table S3.

### Protein expression and purification

The Ddrl expression strains were grown in LB broth to an optical density at 600 nm of 0.6–0.8, followed by adding isopropyl-β-D-thiogalactopyranoside (IPTG) at a final concentration of 0.2 mM. The cells were harvested by centrifugation and resuspended in lysis buffer (20 mM HEPES pH 7.5, 500 mM KCl, 5% glycerol, 1 mM PMSF, and 20 µg/mL lysozyme) and lysed by sonication. After centrifugation, the supernatant was purified by an AKTA Purifier system: The supernatant was loaded onto a HisTrap HP column (GE Healthcare) pre-equilibrated with buffer A (20 mM HEPES pH 7.5, 500 mM KCl, 1 mM TCEP, and 5% glycerol) and finally eluted with 200 mM imidazole. After TEV protease cleavage, the samples were desalted by the HiPrep 26/10 Desalting column (GE Healthcare) with buffer B (20 mM HEPES pH 7.5, 100 mM KCl, 1 mM TCEP, and 5% glycerol). The proteins were subsequently loaded onto HiTrap Q HP column (GE Healthcare) pre-equilibrated with buffer B and eluted with a linear gradient from 100 to 500 mM KCl. The proteins were finally purified by Superdex 75 Increase 10/300 GL column (GE Healthcare) with buffer C (20 mM HEPES pH 7.5, 100 mM KCl, and 1 mM TCEP). Fractions containing the purified proteins were pooled, concentrated, and stored at –80°C. D156Q was expressed and purified by similar methods to those described for wild-type Ddrl.

### Crystallization and structure determination

Ddrl crystals (~15 mg/mL) were grown using the drop vapor diffusion method at 289K over wells containing 0.1 M Bis-Tris pH 6.5, 2.5 M KCl. Cryocooling was achieved by stepwise soaking the crystals in a reservoir solution containing 10%, 20%, and 30% (wt/vol) glycerol. The diffraction intensities were recorded at Shanghai Synchrotron Radiation Facility (Shanghai, China) and were integrated and scaled using the XDS suite (55). The structure was determined by molecular replacement method using SdrP (PDB ID: 2ZCW) as the search model (56). Structures were refined using PHENIX (57) and interspersed with manual model building using COOT (58). Later stages of refinement employed TLS group anisotropic B-factor refinement. All the residues are in the most favorable and allowed regions of the Ramachandran plot. The final model comprises residues 12–202. The statistics for data collection and refinement are listed in Table S1.

### Electrophoretic mobility shift assays

Standard EMSA reaction mixture consisted of 20 mM HEPES pH 7.5, 100 mM NaCl, 20 µg/mL bovine serum albumin (BSA), 1 mM TCEP, 100 nM 5'-Cy5-labeled DNA, and 1–3 µM Ddrl. The reactions could contain 10 µM Mn<sup>2+</sup> and 100 µM cAMP if necessary. The reaction mixture was incubated at 30°C for 30 min, loaded onto 20% (wt/vol) polyacrylamide gels, and run for 80 min at 180 V in 1 × Tris-borate buffer at 4°C (ice-water bath). The gel was then photographed using a Typhoon 9500 (GE Healthcare).

## MST assays

To determine the DNA binding affinity constants, 20 nM Cy5-labeled DNA was incubated with a dilution series of Ddrl (0.305 nM to 10  $\mu$ M) in an MST buffer (20 mM HEPES pH 7.5, 100 mM KCl, and 0.05% Tween 20) for 30 min at room temperature. The reactions could contain 10  $\mu$ M Mn<sup>2+</sup> and 100  $\mu$ M cAMP if necessary. The MST measurements were performed using the Monolith NT.115 instrument (NanoTemper Technologies, München, Germany). For cAMP binding affinity measurements, N-terminal-eGFP fused Ddrl was incubated with a dilution series of cAMP (1.2  $\mu$ M to 2.5 mM) in MST buffer. Data were analyzed using MO.Affinity Analysis software and GraphPad Prism 8. Binding curves represent the change in normalized fluorescence (fraction bound or Fnorm), and  $K_d$  values were calculated using the  $K_d$  Fit Model. All experimental data were obtained from three independent replicates (Table 1).

## Molecular dynamics simulations

We designed our computational model by superimposing our resolved Ddrl dimer structure onto the ecCRP-DNA complex (PDB ID: 2CGP), selectively retaining the cAMP molecules in the second binding site and mutating the DNA sequence into a representative RDRM-mimic (AAATGTTATGTCAAAACATG). For Ddrl protein, the AMBER14SB force field was utilized, while the DNA was modeled using the OL21 force field. The cAMP molecules were parametrized with the Generalized Amber Force Field and assigned AM1-BCC charges. The system was solvated with TIP3P water in a 1-nm buffered cubic box and neutralized with 150 mM NaCl with tleap in AmberTools23. Quantities of ions were calculated by SLTCAP server. A cutoff of 1 nm is applied for non-bonded interactions. The reference temperature and pressure were 310.0K and 1.0 bar, respectively.

Following a 10,000-step steepest descent energy minimization and subsequent 0.5 ns NVT and 0.5 ns NPT equilibrations, we run molecular dynamics simulations for 1,000 ns each round. In the first round, excessive Mn<sup>2+</sup> was added to probe the most probable binding regions, employing the Li-Merz 12-6-4 LJ potential. Four independent MD simulations were performed using Amber22 software. In the second round of simulations, nonspecifically bound Mn<sup>2+</sup> ions were removed from the last frame of each trajectory in the first round and further equilibrated the system by running two independent simulations each. The remaining Mn<sup>2+</sup> ions were parameterized using the Li-Merz 12-6 nonbonded model so that the interaction between Mn<sup>2+</sup> and other molecules was slightly weakened to confirm the stability of Mn<sup>2+</sup> binding. Simulations were performed using Gromacs 2023.2. The coordinates were saved every 0.5 ns. The trajectory visualization and clustering analysis were conducted using VMD 1.9.4a57. The MDAnalysis Python package was used for contact analysis and distance calculation. Effective contact with Mn<sup>2+</sup> ions is defined when O/N/S atoms from at least three protein residues, nucleotides, or the cAMP molecule are within 2.5 Å distance around the Mn<sup>2+</sup> ion.

## ACKNOWLEDGMENTS

The authors would like to thank the staff at the Shanghai Synchrotron Radiation Facility (beamline BL02U1) for assistance in data collection. The authors also thank Jie Ma at the Core Facilities Life Sciences Institute of Zhejiang University for the support of MST experiments.

This work was supported by the National Natural Science Foundation of China (32222001, 12104396, U1967217); the Zhejiang Provincial Natural Science Foundation of China (LDQ23C050002); the National Key Research and Development Program of China (2021YFD1400500, 2021YFF1200404, and 2021YFA1201200); and Starry Night Science Fund at Shanghai Institute for Advanced Study of Zhejiang University (SN-ZJU-SIAS-003).

Y.Z. conceived the project. Y.W. and Y.Z. carried out crystallization and data collection. Y.Z. determined crystal structures and analyzed the data. Y.W., J.H., Y.C., C.C., and S.Y. did biochemical experiments and kinetics analyses. X.G. performed molecular dynamics

simulations. L.W., H.X., D.Z., X.G., M.G., R.Z., and Y.H. took part in data analysis. Y.Z., Y.W., and X.G. wrote the manuscript. All authors discussed the results and commented on the manuscript.

## AUTHOR AFFILIATIONS

<sup>1</sup>MOE Key Laboratory of Biosystems Homeostasis & Protection, Institute of Biophysics, College of Life Sciences, Zhejiang University, Hangzhou, China

<sup>2</sup>Institute of Quantitative Biology, College of Life Sciences, Zhejiang University, Hangzhou, China

<sup>3</sup>Shanghai Institute for Advanced Study, Zhejiang University, Shanghai, China

<sup>4</sup>Department of Chemistry, Columbia University, New York, New York, USA

## AUTHOR ORCIDs

Yudong Wang  <http://orcid.org/0009-0003-9462-135X>

Ye Zhao  <http://orcid.org/0000-0002-5455-2586>

## FUNDING

Funder	Grant(s)	Author(s)
MOST   National Natural Science Foundation of China (NSFC)	32222001	Ye Zhao
MOST   National Natural Science Foundation of China (NSFC)	12104396	Dong Zhang
MOST   National Natural Science Foundation of China (NSFC)	U1967217	Ruhong Zhou
MOST   NSFC   NSFC-Zhejiang Joint Fund   浙江省科学技术厅   Natural Science Foundation of Zhejiang Province (ZJNSF)	LDQ23C050002	Ye Zhao
MOST   National Key Research and Development Program of China (NKPs)	2021YFD1400500	Ye Zhao
MOST   National Key Research and Development Program of China (NKPs)	2021YFF1200404	Dong Zhang
MOST   National Key Research and Development Program of China (NKPs)	2021YFA1201200	Ruhong Zhou

## DATA AVAILABILITY

The coordinate and structure factor have been deposited to the Protein Data Bank with accession code [8YZ7](#).

## ADDITIONAL FILES

The following material is available online.

### Supplemental Material

**Supplemental figures and tables (mBio01144-24-s0001.doc).** Fig. S1 to S2 Tables S1 to S3.

## REFERENCES

- Görke B, Stülke J. 2008. Carbon catabolite repression in bacteria: many ways to make the most out of nutrients. *Nat Rev Microbiol* 6:613–624. <https://doi.org/10.1038/nrmicro1932>
- Nair A, Sarma SJ. 2021. The impact of carbon and nitrogen catabolite repression in microorganisms. *Microbiol Res* 251:126831. <https://doi.org/10.1016/j.micres.2021.126831>
- Walker LM, Haycocks JRJ, Van Kessel JC, Dalia TN, Dalia AB, Grainger DC. 2023. A simple mechanism for integration of quorum sensing and cAMP signalling in *Vibrio cholerae*. *Elife* 12:RP86699. <https://doi.org/10.7554/elife.86699>
- Huang T-P, Wong ACL. 2007. A cyclic AMP receptor protein-regulated cell-cell communication system mediates expression of a FecA

- homologue in *stenotrophomonas maltophilia*. *Appl Environ Microbiol* 73:5034–5040. <https://doi.org/10.1128/AEM.00366-07>
5. Ritzert JT, Minasov G, Embry R, Schipma MJ, Satchell KJF. 2019. The cyclic AMP receptor protein regulates quorum sensing and global gene expression in *Yersinia pestis* during planktonic growth and growth in biofilms. *mBio* 10:e02613-19. <https://doi.org/10.1128/mBio.02613-19>
6. Zou M, Wang K, Zhao J, Lu H, Yang H, Huang M, Wang L, Wang G, Huang J, Min X. 2023. DegS protease regulates the motility, chemotaxis, and colonization of *Vibrio cholerae*. *Front Microbiol* 14:1159986. <https://doi.org/10.3389/fmicb.2023.1159986>
7. Gibson JA, Gebhardt MJ, Santos RERS, Dove SL, Watnick PI. 2022. Sequestration of a dual function DNA-binding protein by *Vibrio cholerae* CRP. *Proc Natl Acad Sci U S A* 119:e2210115119. <https://doi.org/10.1073/pnas.2210115119>
8. Liu C, Sun D, Liu J, Chen Y, Zhou X, Ru Y, Zhu J, Liu W. 2022. cAMP and c-di-GMP synergistically support biofilm maintenance through the direct interaction of their effectors. *Nat Commun* 13:1493. <https://doi.org/10.1038/s41467-022-29240-5>
9. McKay DB, Weber IT, Steitz TA. 1982. Structure of catabolite gene activator protein at 2.9-A resolution. Incorporation of amino acid sequence and interactions with cyclic AMP. *J Biol Chem* 257:9518–9524.
10. Krol E, Werel L, Essen LO, Becker A. 2023. Structural and functional diversity of bacterial cyclic nucleotide perception by CRP proteins. *Microlife* 4:uqad024. <https://doi.org/10.1093/femsml/uqad024>
11. Youn H, Carranza M. 2023. cAMP activation of the cAMP receptor protein, a model bacterial transcription factor. *J Microbiol* 61:277–287. <https://doi.org/10.1007/s12275-023-00028-6>
12. Passner JM, Steitz TA. 1997. The structure of a CAP-DNA complex having two cAMP molecules bound to each monomer. *Proc Natl Acad Sci U S A* 94:2843–2847. <https://doi.org/10.1073/pnas.94.7.2843>
13. Parkinson G, Wilson C, Gunasekera A, Ebright YW, Ebright RH, Berman HM. 1996. Structure of the CAP-DNA complex at 2.5 angstroms resolution: a complete picture of the protein-DNA interface. *J Mol Biol* 260:395–408. <https://doi.org/10.1006/jmbi.1996.0409>
14. Youn H, Koh J, Roberts GP. 2008. Two-state allosteric modeling suggests protein equilibrium as an integral component for cyclic AMP (cAMP) specificity in the cAMP receptor protein of *Escherichia coli*. *J Bacteriol* 190:4532–4540. <https://doi.org/10.1128/JB.00074-08>
15. Gárate F, Dokas S, Lanfranco MF, Canavan C, Wang I, Correia JJ, Maillard RA. 2021. cAMP is an allosteric modulator of DNA-binding specificity in the cAMP receptor protein from *Mycobacterium tuberculosis*. *J Biol Chem* 296:100480. <https://doi.org/10.1016/j.jbc.2021.100480>
16. Stapleton M, Haq I, Hunt DM, Arnvig KB, Artymuk PJ, Buxton RS, Green J. 2010. *Mycobacterium tuberculosis* cAMP receptor protein (Rv3676) differs from the *Escherichia coli* paradigm in its cAMP binding and DNA binding properties and transcription activation properties. *J Biol Chem* 285:7016–7027. <https://doi.org/10.1074/jbc.M109.047720>
17. Lim S, Jung J-H, Blanchard L, de Groot A. 2019. Conservation and diversity of radiation and oxidative stress resistance mechanisms in *Deinococcus* species. *FEMS Microbiol Rev* 43:19–52. <https://doi.org/10.1093/femsre/fuy037>
18. Qi HZ, Wang WZ, He JY, Ma Y, Xiao FZ, He SY. 2020. Antioxidative system of *Deinococcus radiodurans*. *Res Microbiol* 171:45–54. <https://doi.org/10.1016/j.resmic.2019.11.002>
19. Slade D, Radman M. 2011. Oxidative stress resistance in *Deinococcus radiodurans*. *Microbiol Mol Biol Rev* 75:133–191. <https://doi.org/10.1128/MMBR.00015-10>
20. Blanchard L, Guérin P, Roche D, Cruveiller S, Pignol D, Vallenet D, Armengaud J, de Groot A. 2017. Conservation and diversity of the IrrE/DdrO-controlled radiation response in radiation-resistant *Deinococcus* bacteria. *Microbiologyopen* 6:e00477. <https://doi.org/10.1002/mbo3.477>
21. Makarova KS, Omelchenko MV, Gaidamakova EK, Matrosova VY, Vasilenko A, Zhai M, Lapidus A, Copeland A, Kim E, Land M, et al. 2007. *Deinococcus* geothermalis: the pool of extreme radiation resistance genes shrinks. *PLoS One* 2:e955. <https://doi.org/10.1371/journal.pone.0000955>
22. Eugénie N, Zivanovic Y, Lelandais G, Coste G, Bouthier de la Tour C, Bentchikou E, Servant P, Confalonieri F. 2021. Characterization of the radiation desiccation response regulon of the radioresistant bacterium *Deinococcus radiodurans* by integrative genomic analyses. *Cells* 10:2536. <https://doi.org/10.3390/cells10102536>
23. Sugiman-Marangos SN, Weiss YM, Junop MS. 2016. Mechanism for accurate, protein-assisted DNA annealing by *Deinococcus radiodurans* DdrB. *Proc Natl Acad Sci U S A* 113:4308–4313. <https://doi.org/10.1073/pnas.1520847113>
24. de la Tour CB, Mathieu M, Servant P, Coste G, Norais C, Confalonieri F. 2021. Characterization of the DdrD protein from the extremely radioresistant bacterium *Deinococcus radiodurans*. *Extremophiles* 25:343–355. <https://doi.org/10.1007/s00792-021-01233-0>
25. Banneville A-S, Bouthier de la Tour C, De Bonis S, Hognon C, Colletier J-P, Teulon J-M, Le Roy A, Pellequer J-L, Monari A, Dehez F, Confalonieri F, Servant P, Timmins J. 2022. Structural and functional characterization of DdrC, a novel DNA damage-induced nucleoid associated protein involved in DNA compaction. *Nucleic Acids Res* 50:7680–7696. <https://doi.org/10.1093/nar/gkac563>
26. Lu H, Chen Z, Xie T, Zhong S, Suo S, Song S, Wang L, Xu H, Tian B, Zhao Y, Zhou R, Hua Y. 2024. The *Deinococcus* protease PprI senses DNA damage by directly interacting with single-stranded DNA. *Nat Commun* 15:1892. <https://doi.org/10.1038/s41467-024-46208-9>
27. Lu H, Wang L, Li S, Pan C, Cheng K, Luo Y, Xu H, Tian B, Zhao Y, Hua Y. 2019. Structure and DNA damage-dependent derepression mechanism for the XRE family member DG-DdrO. *Nucleic Acids Res* 47:9925–9933. <https://doi.org/10.1093/nar/gkz720>
28. de Groot A, Siponen MI, Magerand R, Eugénie N, Martin-Arevalillo R, Doloy J, Lemaire D, Brandelet G, Parcy F, Dumas R, Roche P, Servant P, Confalonieri F, Arnoux P, Pignol D, Blanchard L. 2019. Crystal structure of the transcriptional repressor DdrO: insight into the metalloprotease/repressor-controlled radiation response in *Deinococcus*. *Nucleic Acids Res* 47:11403–11417. <https://doi.org/10.1093/nar/gkz883>
29. Meyer L, Coste G, Sommer S, Oberto J, Confalonieri F, Servant P, Pasternak C. 2018. DdrI, a cAMP receptor protein family member, acts as a major regulator for adaptation of *Deinococcus radiodurans* to various stresses. *J Bacteriol* 200:e00129-18. <https://doi.org/10.1128/JB.00129-18>
30. Yang S, Xu H, Wang J, Liu C, Lu H, Liu M, Zhao Y, Tian B, Wang L, Hua Y. 2016. Cyclic AMP receptor protein acts as a transcription regulator in response to stresses in *Deinococcus radiodurans*. *PLoS ONE* 11:e0155010. <https://doi.org/10.1371/journal.pone.0155010>
31. Popovych N, Tzeng S-R, Tonelli M, Ebright RH, Kalodimos CG. 2009. Structural basis for cAMP-mediated allosteric control of the catabolite activator protein. *Proc Natl Acad Sci U S A* 106:6927–6932. <https://doi.org/10.1073/pnas.0900595106>
32. Chen H, Xu G, Zhao Y, Tian B, Lu H, Yu X, Xu Z, Ying N, Hu S, Hua Y. 2008. A novel OxyR sensor and regulator of hydrogen peroxide stress with one cysteine residue in *Deinococcus radiodurans*. *PLoS One* 3:e1602. <https://doi.org/10.1371/journal.pone.0001602>
33. Ul Hussain Shah AM, Zhao Y, Wang Y, Yan G, Zhang Q, Wang L, Tian B, Chen H, Hua Y. 2014. A MUR regulator protein in the extremophilic bacterium *Deinococcus radiodurans*. *PLoS One* 9:e106341. <https://doi.org/10.1371/journal.pone.0106341>
34. Daly MJ, Gaidamakova EK, Matrosova VY, Vasilenko A, Zhai M, Venkateswaran A, Hess M, Omelchenko MV, Kostandarites HM, Makarova KS, Wackett LP, Fredrickson JK, Ghosal D. 2004. Accumulation of Mn(II) in *Deinococcus radiodurans* facilitates gamma-radiation resistance. *Science* 306:1025–1028. <https://doi.org/10.1126/science.1103185>
35. Xu Y, Xu L, Qin C, Wang L, Guo J, Hua Y, Zhao Y. 2022. Mechanisms of helicase activated DNA end resection in bacteria. *Structure* 30:1298–1306. <https://doi.org/10.1016/j.str.2022.06.005>
36. Zhang H, Xu Q, Lu M, Xu X, Wang Y, Wang L, Zhao Y, Hua Y. 2014. Structural and functional studies of MutS2 from *Deinococcus radiodurans*. *DNA Repair (Amst)* 21:111–119. <https://doi.org/10.1016/j.dnarep.2014.04.012>
37. Cheng K, Xu H, Chen X, Wang L, Tian B, Zhao Y, Hua Y. 2016. Structural basis for DNA 5'-end resection by RecJ. *Elife* 5:e14294. <https://doi.org/10.7554/elife.14294>
38. Agari Y, Kashihara A, Yokoyama S, Kuramitsu S, Shinkai A. 2008. Global gene expression mediated by *thermus thermophilus* SdrP, a CRP/FNR family transcriptional regulator. *Mol Microbiol* 70:60–75. <https://doi.org/10.1111/j.1365-2958.2008.06388.x>
39. Venkateswaran A, McFarlan SC, Ghosal D, Minton KW, Vasilenko A, Makarova K, Wackett LP, Daly MJ. 2000. Physiologic determinants of

- radiation resistance in *Deinococcus radiodurans*. Appl Environ Microbiol 66:2620–2626. <https://doi.org/10.1128/AEM.66.6.2620-2626.2000>
40. Kamble VA, Rajpurohit YS, Srivastava AK, Misra HS. 2010. Increased synthesis of signaling molecules coincides with reversible inhibition of nucleolytic activity during postirradiation recovery of *Deinococcus radiodurans*. FEMS Microbiol Lett 303:18–25. <https://doi.org/10.1111/j.1574-6968.2009.01855.x>
41. Youn H, Kerby RL, Conrad M, Roberts GP. 2006. Study of highly constitutively active mutants suggests how cAMP activates cAMP receptor protein. J Biol Chem 281:1119–1127. <https://doi.org/10.1074/jbc.M509421200>
42. Frendorf PO, Lauritsen I, Sekowska A, Danchin A, Nørholm MHH. 2019. Mutations in the global transcription factor CRP/CAP: insights from experimental evolution and deep sequencing. Comput Struct Biotechnol J 17:730–736. <https://doi.org/10.1016/j.csbj.2019.05.009>
43. Fiser A, Simon I, Barton GJ. 1996. Conservation of amino acids in multiple alignments: aspartic acid has unexpected conservation. FEBS Lett 397:225–229. [https://doi.org/10.1016/s0014-5793\(96\)01181-7](https://doi.org/10.1016/s0014-5793(96)01181-7)
44. Doig AJ. 2008. Stability and design of alpha-helical peptides. Prog Mol Biol Transl Sci 83:1–52. [https://doi.org/10.1016/S0079-6603\(08\)00601-6](https://doi.org/10.1016/S0079-6603(08)00601-6)
45. Sajadi SAA. 2010. Metal ion-binding properties of L-glutamic acid and L-aspartic acid, a comparative investigation. NS 02:85–90. <https://doi.org/10.4236/ns.2010.22013>
46. Cheng K, Chen X, Xu G, Wang L, Xu H, Yang S, Zhao Y, Hua Y. 2015. Biochemical and functional characterization of the Nura-Hera complex from *Deinococcus Radiodurans*. J Bacteriol 197:2048–2061. <https://doi.org/10.1128/JB.00018-15>
47. Dai J, Gao K, Yao T, Lu H, Zhou C, Guo M, Dai S, Wang L, Xu H, Tian B, Hua Y, Zhao Y. 2020. Late embryogenesis abundant Group3 protein (DrLEA3) is involved in antioxidation in the extremophilic bacterium *Deinococcus radiodurans*. Microbiol Res 240:126559. <https://doi.org/10.1016/j.micres.2020.126559>
48. Zhao Y, Lu M, Zhang H, Hu J, Zhou C, Xu Q, Ul Hussain Shah AM, Xu H, Wang L, Hua Y. 2015. Structural insights into catalysis and dimerization enhanced exonuclease activity of RNase J. Nucleic Acids Res 43:5550–5559. <https://doi.org/10.1093/nar/gkv444>
49. Hicks MN, Gunasekara S, Serate J, Park J, Mosharaf P, Zhou Y, Lee JW, Youn H. 2017. Gly184 of the *Escherichia coli* cAMP receptor protein provides optimal context for both DNA binding and RNA polymerase interaction. J Microbiol 55:816–822. <https://doi.org/10.1007/s12275-017-7266-x>
50. Feng Y, Zhang Y, Ebright RH. 2016. Structural basis of transcription activation. Science 352:1330–1333. <https://doi.org/10.1126/science.aaf4417>
51. Liu B, Hong C, Huang RK, Yu Z, Steitz TA. 2017. Structural basis of bacterial transcription activation. Science 358:947–951. <https://doi.org/10.1126/science.aoa1923>
52. Wang J, Tian Y, Zhou Z, Zhang L, Zhang W, Lin M, Chen M. 2016. Identification and functional analysis of RelA/SpoT homolog (RSH) genes in *Deinococcus radiodurans*. J Microbiol Biotechnol 26:2106–2115. <https://doi.org/10.4014/jmb.1601.01017>
53. Pomp W, Meeussen JVW, Lenstra TL. 2024. Transcription factor exchange enables prolonged transcriptional bursts. Mol Cell 84:1036–1048. <https://doi.org/10.1016/j.molcel.2024.01.020>
54. Dorman CJ, Schumacher MA, Bush MJ, Brennan RG, Buttner MJ. 2020. When is a transcription factor a NAP? Curr Opin Microbiol 55:26–33. <https://doi.org/10.1016/j.mib.2020.01.019>
55. Kabsch W. 2010. Xds. Acta Crystallogr D Biol Crystallogr 66:125–132. <https://doi.org/10.1107/S0907444909047337>
56. McCoy AJ, Grosse-Kunstleve RW, Adams PD, Winn MD, Storoni LC, Read RJ. 2007. Phaser crystallographic software. J Appl Crystallogr 40:658–674. <https://doi.org/10.1107/S0021889807021206>
57. Adams PD, Afonine PV, Bunkóczki G, Chen VB, Davis IW, Echols N, Headd JJ, Hung L-W, Kapral GJ, Grosse-Kunstleve RW, McCoy AJ, Moriarty NW, Oeffner R, Read RJ, Richardson DC, Richardson JS, Terwilliger TC, Zwart PH. 2010. PHENIX: a comprehensive python-based system for macromolecular structure solution. Acta Crystallogr D Biol Crystallogr 66:213–221. <https://doi.org/10.1107/S0907444909052925>
58. Emsley P, Lohkamp B, Scott WG, Cowtan K. 2010. Features and development of coot. Acta Crystallogr D Biol Crystallogr 66:486–501. <https://doi.org/10.1107/S0907444910007493>